Physics – Uspekhi **61** (8) 793 – 804 (2018) ©2018 Uspekhi Fizicheskikh Nauk, Russian Academy of Sciences

CONFERENCES AND SYMPOSIA

PACS numbers: 96.50.Ci, 96.50.Ek, 96.60.Vg

Global structure of the heliosphere: 3D kinetic-MHD model and the interpretation of spacecraft data

V V Izmodenov

DOI: https://doi.org/10.3367/UFNe.2017.04.038293

Contents

Abstract. This paper is a brief overview of research into the interaction between the solar wind and local interstellar medium. This interaction determines the global structure of the heliosphere (the region occupied by the solar wind) and has a complex multicomponent character. We describe the three-dimensional kinetic-magnetohydrodynamic model of the interaction, which includes plasma and neutral components of the interstellar medium and solar wind, the heliospheric and interstellar magnetic fields, and the latitudinal and temporal variations of solar wind parameters. In describing the results, magnetic-field-related effects are given special attention, in particular, the magnetic-field-driven plasma depletion in the vicinity of the heliopause. The model explains a sufficiently large body of data from Voyager-1 and Voyager-2, the Interstellar Boundary Explorer (IBEX), the Solar and Heliospheric Observatory (SOHO), the Hubble Space Telescope (HST), and other spacecraft. Based on the experimental data and using the model, the parameters of the interstellar medium and of the interstellar magnetic field are determined. It is shown, however, that a single model using a single set of boundary conditions cannot self-consistently explain all the data available. The Voyager-1 data on the scattered solar Lyman-alpha radiation is taken as an example to illustrate the difficulties that arise.

Keywords: solar wind, interstellar medium, interstellar atoms, magnetohydrodynamics, shock waves

V V Izmodenov Space Research Institute, Russian Academy of Sciences, ul. Profsoyuznaya 84/32, 117997 Moscow, Russian Federation;
Lomonosov Moscow State University,
Leninskie gory 1, 119991 Moscow, Russian Federation;
National Research University "Higher School of Economics",
ul. Myasnitskaya 20, 101000 Moscow, Russian Federation
E-mail: izmod@iki.rssi.ru

Received 26 January 2018
Uspekhi Fizicheskikh Nauk **188** (8) 881 – 893 (2018)
DOI: https://doi.org/10.3367/UFNr.2017.04.038293
Translated by M Zh Shmatikov; edited by A M Semikhatov

1. Introduction

The heliosphere is the region occupied by the solar wind. The solar wind is an extension of the solar corona, the Sun's upper atmosphere. The corona temperature is of the order of 10^6 K. Owing to this, first, the gas in the corona is fully ionized and, second, some particles in this gas have velocities large enough to overcome the Sun's gravitation force. It is those high-velocity particles that form the solar wind, the solar-plasma flux that fills interstellar space. At large heliocentric distances, the solar wind is a supersonic flow. In Earth's orbit, the solar-wind Mach number is $\sim 5-10$. Solar wind parameters are not invariable and depend on the location of the wind outflow from the Sun (see, e.g., [1]) and hence on the solar cycle and heliolatitude.

At large heliocentric distances [$\sim$ 100 astronomic units (a.u.)], the solar wind interacts with the interstellar medium that surrounds the Sun. The Sun is located at the edge of a spiral arm of our Galaxy (the Orion Arm) and rotates together with other stars and interstellar wind around the Galaxy center with a velocity $\sim$230 km s^{-1}. The distance between the Sun and the Galaxy center is of the order of 26,000 light years. However, to determine the structure of the heliospheric boundary, we need to know the properties of the interstellar medium at significantly smaller characteristics distances, of the order of one or several parsecs. Owing to spectroscopic studies, the properties of the near-Sun interstellar medium are known sufficiently well. Currently, the Sun is located at the boundary of a minor interstellar cloud referred to as the Local Interstellar Cloud (LIC). The cloud, which is several parsecs in diameter, belongs to a small group of interstellar clouds close to us that have temperatures of $(5–10)\times10^3$ K and concentrations of the order of 0.1–0.3 cm^{-3}. The entire group of local clouds is believed to be contained within a hypothetical Local Bubble, the interstellar space region with a characteristic size of the order of 100 ps filled with hot ionized plasma with a temperature of the order of 1 mln K. According to a hypothesis, the Local Bubble appeared as a result of the burst of a supernova (or several supernovae) about 1 bln years ago.

Spectroscopic studies show that the Sun is located virtually on the LIC boundary. Its closest neighbor is the G-cloud. Currently, it is not known whether the LIC and G-cloud border each other or are separated by a hot plasma area of the Local Bubble into which both are embedded. During the next 3,000 years, the Sun will leave the LIC and move to either the neighboring G-cloud or the hot plasma of the Local Bubble.

We note that the Sun moves with respect to the LIC. The LIC velocity (with respect to the Sun) and its temperature can be determined by measuring parameters of the interstellar helium atoms that have large mean free paths and penetrate into the heliosphere, where they can be measured by spacecraft. Fluxes of interstellar helium atoms were measured by the Ulysses and IBEX (Interstellar Boundary Explorer) spacecraft: the velocity of the relative motion of the LIC is ~ 26.4 km s^{-1}, and its temperature is about 6,400 K (see, e.g., [2, 3] and the references therein).

In 1961, Parker proposed the first hydrodynamic models for the solar wind interaction with the interstellar medium. He theoretically considered three cases: (1) the outflow of a hypersonic stellar wind into the interstellar gas at rest; (2) the outflow of the hypersonic stellar wind into an essentially subsonic (Mach number $M \ll 1$) flow of the interstellar medium; and (3) the outflow of the hypersonic stellar wind into a uniform interstellar magnetic field.

A gasdynamic model of the solar wind interaction with a hypersonic flow of interstellar gas was proposed in [5]. A qualitative picture of the flow obtained in [5] is shown in Fig. 1a. The contact discontinuity referred to as the *heliopause* separates the solar wind from the interstellar medium. The heliopause can be considered an obstacle flown around by the fluxes of the solar wind and interstellar medium, on the respective inner and outer sides. Because the model assumes that both fluxes are supersonic, two shock waves are created: the head shock wave in the interstellar medium and the heliospheric one in the solar wind. The existence of the heliospheric shock wave and the heliopause has now been confirmed with the data collected by the Voyager-1 and 'Voyager-2' spacecraft. The existence of the head shock wave is challenged.

The region of the solar wind interaction with the local interstellar medium is often referred to as the heliospheric interface region and sometimes simply as the heliosphere boundary. The region between two shock waves is referred to as the heliospheric shock layer. A differentiation is made between the internal (between the heliospheric shock wave and heliopause) and external (between the heliopause and head shock wave) shock layers.

In the early 1970s, experiments on scattered solar radiation at wavelengths $\lambda = 1216$ and 584 Å [6–8] proved the existence of interstellar hydrogen and helium atoms moving in near-solar space. In 1975, it was shown in [9] that the charged and neutral components can affect each other both in the shock layer area and inside the heliosphere. The most efficient mechanism of interaction between the charged and neutral components is the charge-exchange reaction ($H^+ + H = H + H^+$). This interaction has two features. First, the shock layer region (the region between the heliospheric shock wave (TS) and external shock wave (BS) in Fig. 1) is a kind of filter for interstellar hydrogen atoms that penetrate into the Solar System from the interstellar medium. Second, resonance charge exchange can affect the flow of the charged component, the structure of the interaction area, and, in particular, the distance from this area to the Sun. Figures 1b, c show the dynamic effect of hydrogen atoms on the location of the shock waves (DS and TS) and the heliopause (HP). Due to this effect, the heliospheric interface shifts closer to the Sun. The shape of the heliospheric shock wave becomes closer to a sphere. The Mach disc and the complex shock structure in the tail region, which consists of a reflected shock wave (RS) and tangential discontinuity, vanish. A detailed discussion of these effects can be found, e.g., in [10].

A self-consistent model of the solar wind interaction with the two-component (plasma and H atoms) local interstellar medium (LISM) was developed for the first time in [11]. In that axial-symmetric model, the interstellar wind was regarded as a plane-parallel uniform flow, and the solar wind as a supersonic spherically symmetric flow in Earth's orbit. For such boundary conditions, the plasma flow in the heliospheric interface is axially symmetric. It was assumed in the model that the charged and neutral components interact primarily by charge exchange. The model also includes photo ionization, solar gravity, and radiation pressure, which affect the distribution of H atoms in the vicinity (10–15 a.u.) of the Sun.

The neutral component was described using the kinetic approach, because the mean free path of hydrogen atoms is comparable to the characteristic dimension of the heliosphere (see, e.g., [12]). For the charged component, Euler gasdynamic equations were solved with source terms that take momentum and energy exchange in the process of charge exchange into account. The source terms were calculated using the Monte Carlo method with splitting trajectories [13]. In the 1990s and 2000s, this model was adopted as the 'standard' one, and it has been improved by including various physical processes and components. For example, in [14, 15], the effect of galactic and anomalous components of cosmic rays was studied. The evolution of the hydrogen atom distribution function as part of the axial-symmetric model was analyzed in [16]. The dynamic effect of interstellar helium ions and solar alpha particles was studied in [17]. Propagation of interstellar oxygen and nitrogen atoms through the heliospheric shock wave region was considered in [18, 19]. The axial-symmetric two-component model was extended in [20] to the tail region up to distances of 30,000 a.u. Nonstationary effects related to the 11-year solar activity cycle were studied in [21, 22]. Effects of interstellar magnetic fields were studied in [23]. The results obtained prior to 2009 are reviewed in [24].

In 2015, the next step in developing the kinetic magnetohydrodynamic (MHD) model of solar wind interaction with the local interstellar medium was made in [25]. The model developed in [25] enables explaining the bulk of the experimental data obtained by different spacecraft. In Section 2, the mathematical formulation of the problem in [25] and some important results are presented. An application of that model to the analysis of spacecraft data is discussed in Section 3.

2. Modern kinetic magnetohydrodynamic model of solar wind interaction with the interstellar medium

2.1 Problem formulation

The model presented in [25] is a 3D nonstationary kinetic MHD model. In the model, the interstellar medium is assumed to be a partly ionized medium that includes two

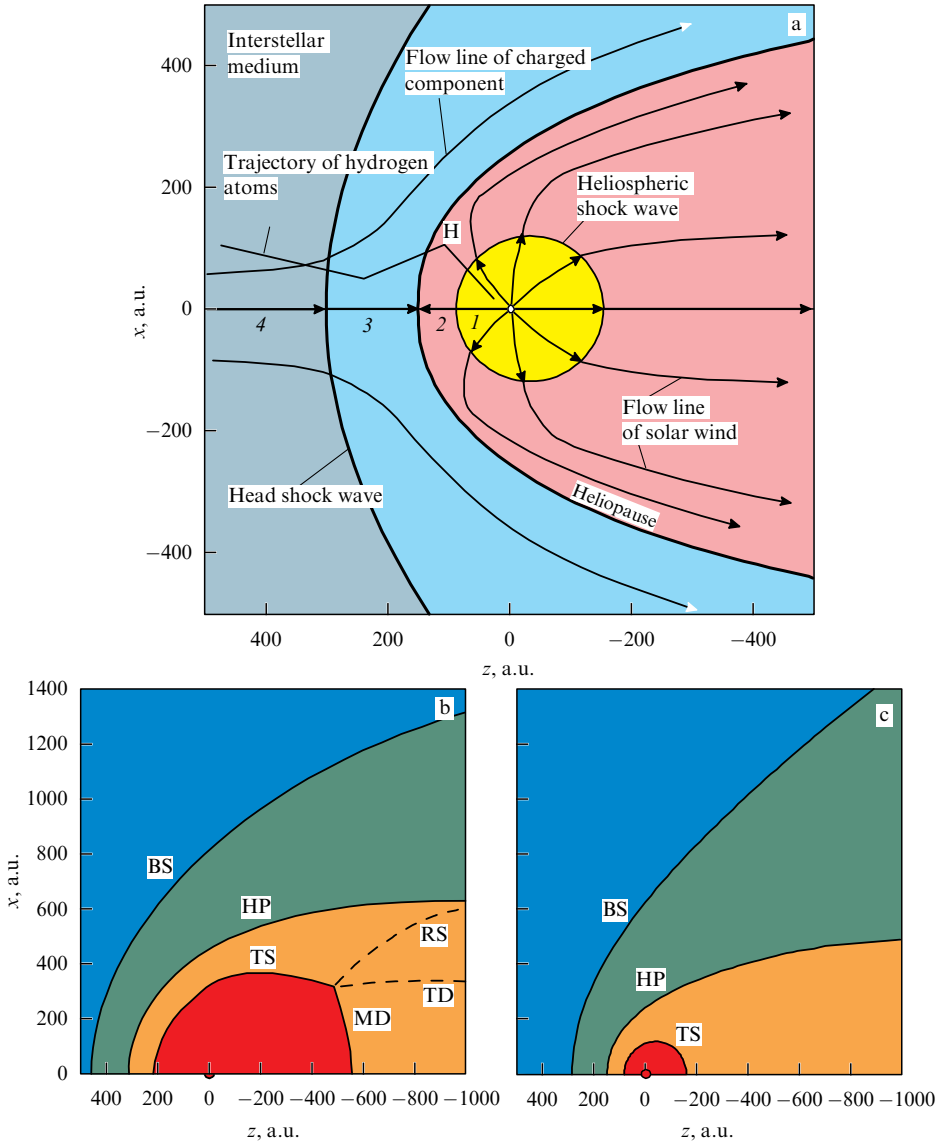

Figure 1. (a) Heliospheric interface is the region where the solar wind interacts with the interstellar medium. The heliopause is the interface surface that separates solar-wind plasma from interstellar plasma. The solar wind is decelerated in the heliospheric shock wave from a supersonic speed to a subsonic speed (provided $n_{\mathrm{H,LIC}} \neq 0$). In the external shock wave, the interstellar medium flux is decelerated and heated. The heliospheric interface region may be divided into four sub-regions featuring different characteristics of plasma: *1* denotes the supersonic solar wind, *2* denotes the subsonic solar wind between the heliopause and heliospheric shock wave (this region will be referred to as the internal shock layer), *3* denotes the perturbed interstellar plasma between the heliopause and the external shock wave (this region will be referred to as the external shock layer), *4* denotes the supersonic flux of the interstellar medium. The effect of interstellar hydrogen atoms on the dimension and structure of the heliospheric interface: the heliospheric interface in the case of a completely (b) and partially (c) ionized interstellar medium (results of calculations in model [11] are presented). BS is the external shock wave; HP is the heliopause, TS is the heliospheric shock wave, MD is the Mach disc, TD is tangential discontinuity, and RS is the reflected shock wave.

components: (1) a neutral component consisting of hydrogen atoms and (2) a charged (plasma) component consisting of protons, electrons, and helium ions. The solar wind plasma is assumed to consist of protons, alpha particles, and electrons. The model also assumes that captured protons are immediately and completely assimilated in thermal plasma. This assumption is essential. As shown in [26], the assimilation of captured protons with thermal velocities does not occur instantaneously, and the captured protons must be described within the kinetic approximation.

Because the mean free path of hydrogen atoms is comparable to or greater than the characteristic dimension of the problem (see, e.g., [12]), the kinetic approach is used to describe the neutral component, and the $f_{\mathrm{H}}(t, \mathbf{r}, \mathbf{w}_{\mathrm{H}})$ distribution functions is found from the solution of the kinetic equation

$$\frac{\partial f_{\mathrm{H}}}{\partial t} + \mathbf{w}_{\mathrm{H}} \frac{\partial f_{\mathrm{H}}}{\partial \mathbf{r}} + \frac{\mathbf{F}_{\mathrm{r}} + \mathbf{F}_{\mathrm{g}}}{m_{\mathrm{H}}} \frac{\partial f_{\mathrm{H}}}{\partial \mathbf{w}_{\mathrm{H}}} = -\nu_{\mathrm{ph}} f_{\mathrm{H}}(t, \mathbf{r}, \mathbf{w}_{\mathrm{H}})$$

$$- f_{\mathrm{H}} \int |\mathbf{w}_{\mathrm{H}} - \mathbf{w}_{\mathrm{p}}| \, \sigma_{\mathrm{ex}}^{\mathrm{HP}}\left(|\mathbf{w}_{\mathrm{H}} - \mathbf{w}_{\mathrm{p}}|\right) f_{\mathrm{p}}(t, \mathbf{r}, \mathbf{w}_{\mathrm{p}}) \, \mathrm{d}\mathbf{w}_{\mathrm{p}} \qquad (1)$$

$$+ f_{\mathrm{p}}(t, \mathbf{r}, \mathbf{w}_{\mathrm{H}}) \int |\mathbf{w}_{\mathrm{H}}^{*} - \mathbf{w}_{\mathrm{H}}| \, \sigma_{\mathrm{ex}}^{\mathrm{HP}}\left(|\mathbf{w}_{\mathrm{H}}^{*} - \mathbf{w}_{\mathrm{H}}|\right) f_{\mathrm{H}}(t, \mathbf{r}, \mathbf{w}_{\mathrm{H}}^{*}) \, \mathrm{d}\mathbf{w}_{\mathrm{H}}^{*} .$$

Here, $\mathbf{F}_{\mathrm{r}}$ and $\mathbf{F}_{\mathrm{g}}$ are the respective solar pressure and solar force of gravity. They significantly affect the distribution function of interstellar hydrogen atoms inside the heliosphere

at distances less than 10–20 a.u. from the Sun (see, e.g., [27]), while at longer distance the effect of those forces is not large. The term $f_{\rm p}(t,\mathbf{r},\mathbf{w}_{\rm p})$ is the local Maxwell distribution function of protons (of both the solar wind and the interstellar medium) that is determined by gasdynamic parameters: the density $\rho(t,\mathbf{r})$, the velocity $\mathbf{V}(t,\mathbf{r})$, and the temperature $T(t,\mathbf{r})$; $\sigma_{\rm ex}^{\rm HP}(u)$ is the effective cross section of charge exchange of hydrogen atoms and protons, which depends on the absolute value of their relative velocity: $\sigma_{\rm ex}^{\rm HP}(u)=(2.2835\times10^{-7}-1.062\times10^{-8}\ln u)^2$ cm^2 [28], where u is the relative velocity of the atom and the proton measured in cm s^{-1}; $\nu_{\rm ph}=1.67\times10^{-7}(R_{\rm E}/R)^2$ s^{-1} is the photo ionization rate; and $R_{\rm E}$ is 1 a.u.

The charged component is described as an ideal perfect gas with infinite conductivity that does not conduct heat. The MHD equations then take the form

$$\frac{\partial\rho}{\partial t}+\nabla(\rho\mathbf{V})=q_1\,, \tag{2}$$

$$\frac{\partial\rho\mathbf{V}}{\partial t}+\left[\rho\mathbf{V}\otimes\mathbf{V}+\left(p+\frac{B^2}{8\pi}\right)\mathbf{I}-\frac{\mathbf{B}\otimes\mathbf{B}}{4\pi}\right]=\mathbf{q}_2\,, \tag{3}$$

$$\frac{\partial\mathbf{B}}{\partial t}+(\mathbf{V}\otimes\mathbf{B}-\mathbf{B}\otimes\mathbf{V})=0\,,\quad \nabla\mathbf{B}=0\,, \tag{4}$$

$$\frac{\partial E}{\partial t}+\nabla\left[\left(E+p+\frac{B^2}{8\pi}\right)\mathbf{V}-\frac{(\mathbf{VB})}{4\pi}\,\mathbf{B}\right]=q_3\,, \tag{5}$$

where $\mathbf{B}$ is the magnetic field induction vector, $\otimes$ is the operator of the vector tensor product, $\mathbf{I}$ is the unit tensor, $E=\rho V^2/2+p/(\gamma-1)+B^2/(8\pi)$ is the total energy, and $\gamma=5/3$ is the adiabatic exponent. The plasma density is $\rho=m_{\rm p}n_{\rm p}+m_{\rm He}n_{\rm He}$, where $n_{\rm He}$ is the density of helium ions He^+ in the interstellar medium and the density of alpha-particles He^{++} in the solar wind. To determine the density of those two components, additional continuity equations are solved for helium ions in the interstellar medium and for alpha particles in the solar wind. Next, the concentration of protons $n_{\rm p}=(\rho-m_{\rm He}n_{\rm He})/m_{\rm p}$ is determined; p is the thermal pressure of the plasma component given by the sum of partial pressures of the components $p=(2n_{\rm p}+3n_{\rm He^{++}})\,k_{\rm B}T_{\rm p}$ in the solar wind and $p=2(n_{\rm p}+n_{\rm He^{+}})\,k_{\rm B}T_{\rm p}$ in the interstellar medium; $T_{\rm p}$ is the plasma component temperature; and $k_{\rm B}$ is the Boltzmann constant.

The effects of proton charge exchange on interstellar hydrogen atoms and of photo ionization are taken into account in the source terms q_1, $\mathbf{q}_2$, and q_3 in the right-hand sides of MHD equations. The source terms expressed as integrals of atom distribution functions are calculated using the Monte Carlo method:

$$q_1=m_{\rm p}n_{\rm H}\nu_{\rm ph}\,,\quad n_{\rm H}(\mathbf{r},t)=\int f_{\rm H}(t,\mathbf{r},\mathbf{w}_{\rm H})\,{\rm d}\mathbf{w}_{\rm H}\,, \tag{6}$$

$$\mathbf{q}_2=\int m_{\rm p}\nu_{\rm ph}\mathbf{w}_{\rm H}f_{\rm H}(t,\mathbf{r},\mathbf{w}_{\rm H})\,{\rm d}\mathbf{w}_{\rm H}+\iint m_{\rm p}\nu_{\rm rel}\sigma_{\rm ex}^{\rm HP}(\nu_{\rm rel})\times(\mathbf{w}_{\rm H}-\mathbf{w})f_{\rm H}(t,\mathbf{r},\mathbf{w}_{\rm H})f_{\rm p}(t,\mathbf{r},\mathbf{w})\,{\rm d}\mathbf{w}_{\rm H}\,{\rm d}\mathbf{w}\,, \tag{7}$$

$$q_3=\int m_{\rm p}\nu_{\rm ph}\frac{w_{\rm H}^2}{2}f_{\rm H}(t,\mathbf{r},\mathbf{w}_{\rm H})\,{\rm d}\mathbf{w}_{\rm H}+\frac{1}{2}\iint m_{\rm p}\nu_{\rm rel}\sigma_{\rm ex}^{\rm HP}(\nu_{\rm rel})\times(w_{\rm H}^2-w^2)f_{\rm H}(t,\mathbf{r},\mathbf{w}_{\rm H})f_{\rm p}(t,\mathbf{r},\mathbf{w})\,{\rm d}\mathbf{w}_{\rm H}\,{\rm d}\mathbf{w}+n_{\rm H}\nu_{\rm ph}E_{\rm ph}\,. \tag{8}$$

Here, $\nu_{\rm rel}=|\mathbf{w}_{\rm H}-\mathbf{w}|$ is the relative velocity of the atom and the proton, and $E_{\rm ph}$ is the average energy released in photo ionization (4.8 eV).

The source terms in (6)–(8) are calculated simultaneously with solving kinetic equation (1) by the Monte Carlo method with splitting trajectories [13]. In implementing this method, it is assumed that the proton distribution function is a local Maxwellian function; in [13], a generalization of that method to the case of an arbitrary locally isotropic distribution function is proposed.

To complete the problem setup, we fix the boundary conditions. Inner boundary conditions are specified inside the heliosphere, in the area where the solar wind is not perturbed by interaction with the interstellar medium. As the inner boundary, we selected Earth's orbit (more accurately, 1 a.u.). In [25], the problem under consideration was solved in a stationary formulation; therefore, the solar wind parameters on that boundary in the ecliptic plane were determined by temporal smoothing of data on the solar wind parameters obtained from NASA's OMNI-2 database (OMNI is the abbreviation for Operating Missions as Nodes on the Internet). The model also takes the dependence of solar wind parameters on heliolatitude into account (Fig. 2). To calculate the heliolatitude dependence of the speed and density of the particles, we used data on interstellar radio oscillations (see [29]) and scattered solar Lyman-alpha radiation obtained by the SWAN (Solar Wind ANisotropie) device aboard the SOHO (Solar and Heliospheric Observatory) spacecraft [30–32]. We note that maxima of the dynamic pressure of the solar wind occur at medium heliolatitudes (see Fig. 2). Nonstationary formulations of the problems were discussed in [20, 21].

In the model under consideration, the heliospheric magnetic field is assumed to be 'frozen' into the solar wind plasma. It was assumed that on the inner boundary, the magnetic field components correspond to Parker's classical solution [33]:

$$B_{\rm R}=\pm B_{\rm E}\left(\frac{R_{\rm E}}{R}\right)^2\,,\quad B_\theta=0\,,\quad B_\varphi=-\beta_{\rm s}B_{\rm R}\left(\frac{R}{R_{\rm E}}\right)\sin\theta\,. \tag{9}$$

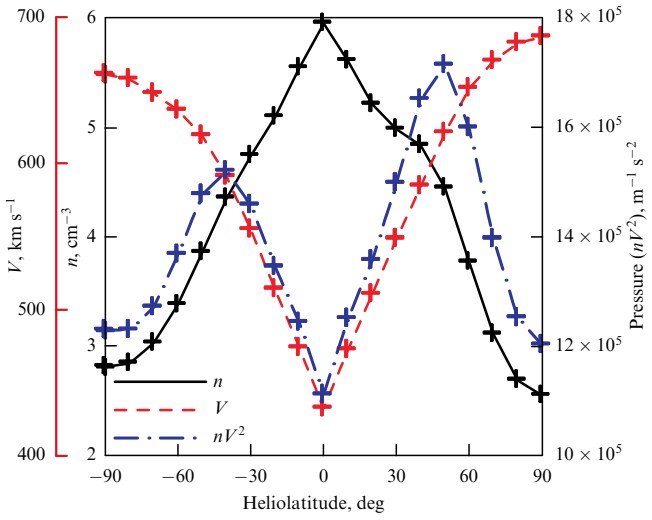

Figure 2. Density n, velocity V, and dynamic pressure nV^2 of the solar wind as a function of heliolatitude.

Here, R, θ, and φ are spherical coordinates related to the solar equatorial plane: θ is the solar latitude measured in the direction from the North Pole (0°) to the South Pole (180°). At $R = R_E = 1$ a.u., we have $B_E = 37.5$ μG and $\beta_s = \Omega R_E / V \approx 1$, with the solar wind velocity $V = 432$ km s^{-1}, Ω is the angular speed of the Sun's rotation around its axis (≈ 25 days), and φ is the solar longitude.

The sign of the radial component B_R at this spatial point depends on the location of the heliospheric current layer and can change with time. But because terms in the ideal-MHD equation that incorporate the magnetic field do not depend on the field polarity, the solution of the problem must be independent of the sign of B_R. The current layer in ideal MHD is an MHD discontinuity where the sign of the magnetic field reverses. We note that this assumption is well confirmed by Voyager data [34], which show that the field rapidly changes its polarity when the spacecraft crosses the current layer, indicating that its thickness is small.

We also note that in ideal MHD, magnetic field lines of the heliospheric and interstellar fields cannot reconnect on the heliopause. This is a good test for numerical models (and is not observed in a number of models under development by other groups). In the model under consideration, there is no problem of reconnection on the heliopause due to numerical effects, because the heliopause is treated as a tangential discontinuity on both sides of which the condition $B_n = 0$ is satisfied. In calculations, this discontinuity area is separated by a numerical mesh. Details of the numerical method and mesh can be found in [25].

Interstellar medium parameters. The outer boundary conditions are set in the unperturbed interstellar medium. In [25], a sphere with a radius of ~ 1000 a.u. was used as the outer boundary.

As was noted in the Introduction, the velocity V of relative motion of the interstellar medium and its temperature are known rather well. It was assumed in [25] that $V_{LISM} = = 26.4$ km s^{-1} and $T_{LISM} = 6530$ K, as follows from the analysis of measurements of interstellar helium atoms made by the Ulysses spacecraft (GAS device) [2, 35–37]. The relative velocity $\mathbf{V}_{LISM}$ of the interstellar medium has the following direction in the heliographic inertial coordinate system HGI 2000: longitude $-1.02°$ and latitude $-5.11°$.

The remaining parameters of the interstellar medium, namely, the density of hydrogen atoms, protons, and helium ions and the value and direction of the magnetic induction vector, are not known to this accuracy and can be considered free parameters. There are no direct measurements of the interstellar medium unperturbed by interaction with the solar wind: although Voyager-1 crossed the heliopause in 2013 at a distance of 122 a.u., it still remains in the area of the perturbed interstellar medium. The values of the parameters listed above can be evaluated by analyzing indirect measurements and using the results of multiparameter model calculations. An analysis of this kind was done in [23, 28]. In [25], the following values of the interstellar medium parameters are chosen: $n_{H,LISM} = 0.14$ cm^{-3}, $n_{p,LISM} = 0.04$ cm^{-3} and $n_{He^+,LISM} = 0.003$ cm^{-3}. The interstellar magnetic field induction was assumed to be $B_{LISM} = 4.4$ μG. The angle between the vectors of the interstellar medium velocity and the interstellar magnetic field induction is $\alpha = 20°$. It was also assumed that the plane defined by the vectors $\mathbf{V}_{LISM}$ and $\mathbf{B}_{LISM}$ coincides with the plane defined by the velocity vectors of the interstellar helium and hydrogen atoms, the latter velocity being known from the analysis of data on scattered (on interstellar hydrogen atoms) solar Lyman-alpha radiation that were obtained by the SWAN device aboard the SOHO spacecraft (see [27, 39]).

The reasons for selecting those values of free parameters are discussed in Section 3. For those values of the parameters, the interstellar medium is a supersonic sub-Alfvén flow. The Mach numbers calculated using the sonic speed, the Alfvén velocity, and the fast magnetic sound velocity (in the direction of interstellar medium motion) are $M = 2.17$, $M_A = 0.631$, and $M_{Z+,LISM} = 0.628$.

2.2 Results of the model

2.2.1 Reference frame. We define a heliocentric reference frame that is convenient for presenting the results. We link it to the velocity and magnetic field induction vectors $\mathbf{V}_{LISM}$ and $\mathbf{B}_{LISM}$. We direct the z axis opposite to the vector of the interstellar medium velocity and select the x axis in the plane defined by $\mathbf{V}_{LISM}$ and $\mathbf{B}_{LISM}$ (the BV plane) and perpendicular to the z axis. To be more specific, we select the positive direction of the x axis such that the projection of the magnetic field induction vector on that axis is negative. The y axis is directed such that the coordinate system is a right-hand one. In the chosen reference frame, the direction to the solar north pole is set by the unit vector with the coordinates (0.6696, −07373, 0.089).

2.2.2 Effect of the interstellar magnetic field. Figures 3–5 show results of calculations done in model [25]. In Fig. 3a, density isolines and flow lines of plasma components (in the zx plane) are plotted, and in Fig. 3c isolines and field lines are shown for the model where the effect of the heliospheric magnetic field is ignored and the solar wind is assumed to be isotropic over heliolatitude. As follows from Fig. 3, it is the interstellar magnetic field that gives rise to the asymmetric global structure of the heliosphere (for comparison, see the results of axial symmetric models in Fig. 1). Manifested the most strongly is the heliopause asymmetry in the upper hemisphere, much farther from the Sun than in the lower hemisphere. The heliocentric distance to the heliopause (HP) depends on the relation between magnetic pressure and the magnetic field strength. The pressure of the interstellar magnetic field attains a maximum in the lower hemisphere, where the magnetic field lines are parallel to the heliopause surface.

If the heliopause shape and location change, the shape of the heliospheric shock wave (TS) also changes. It also becomes asymmetric with respect to the z axis, coming closer to the Sun in the lower hemisphere and going farther away from it in the upper one. It is because of the interstellar magnetic field that Voyager-2 crossed the heliospheric shock wave 10 a.u. closer to the Sum than Voyager-1 did, although the angle between the vector of Voyager-2 motion and the z axis direction (i.e., the direction opposite to the interstellar medium velocity) is significantly larger that the corresponding angle for the Voyager-1 direction. In the case of an axially symmetric heliosphere, the distance to the heliospheric shock wave might be expected to be larger in the Voyager-2 direction. We also note that for the chosen values of the interstellar magnetic field, there is no head shock wave. For fields with a lower strength (~ 2.5 μG), there is a shock wave, but it is weak and located at a significant distance from the heliopause (i.e., it essentially degenerates into a characteristic) [21].

Due to the heliopause asymmetry, the interstellar plasma density in the upper hemisphere ($x > 0$) is larger than in the

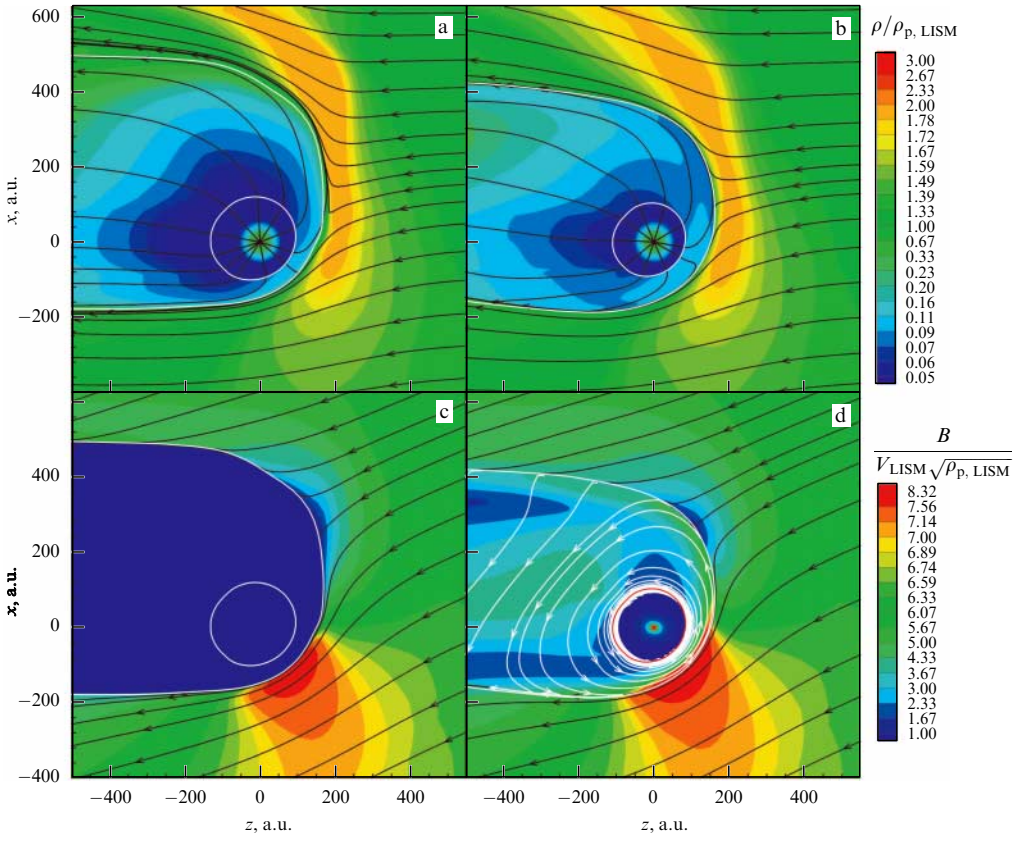

Figure 3. (Color online.) (a, b) Flow lines and density isolines of the plasma component. The density is normalized to the density of protons in the interstellar medium. (c, d) Field lines and isolines of the absolute value of the magnetic field are presented in dimensionless units. Figures a and c show results of calculations without the effect of the heliospheric magnetic field, and Figs b and d, with the field effect taken into account. The results are plotted in the zx plane that is determined by the vectors of the velocity and magnetic field of the interstellar medium.

lower one ($x < 0$), and the stagnation point moves upward along the axis. In the vicinity of that point, the density of the plasma component of the interstellar medium attains a maximum, and the velocity vector has a large V_x component. Because the velocities of interstellar hydrogen atoms produced in that region as a result of charge exchange correspond to the velocities of protons that are their charge-exchange partners, the neutral component also has a nonzero velocity component along the x axis. In [25], the vector $\mathbf{V}_{\mathrm{H}}$ of the average velocity of hydrogen atoms was calculated as a moment of their distribution function. Its x-component is nonzero even at small heliocentric distances. The angle between the average velocity of hydrogen atoms within the heliosphere and the direction of motion of the interstellar medium was calculated to be 3–5° (see [21, 27]). The same deviation of the direction of motion of hydrogen atoms was found in measurements of scattered solar radiation in the Lyman-alpha line by the SOHO spacecraft [31, 39].

2.2.3 Effect of the heliospheric magnetic field. Region of plasma expulsion by the magnetic field. Figures 3b, d show results calculated with the heliospheric magnetic field taken into account. We can see that neither the global structure of the heliosphere nor the spatial distributions of plasma and the magnetic field in the interstellar medium experience qualitative changes. However, a detailed study shows, for example, that the heliocentric distance to the shock wave decreases by ~ 10 a.u. (which corresponds to about three years of flight for Voyager). The quantitative effect of the heliospheric magnetic field is shown in Fig. 4, where 1D distributions of the parameters of plasma and the magnetic field along the z axis are plotted.

A detailed physical explanation of the results obtained is given in [25]. Here, we only note an interesting and important effect of plasma expulsion (decrease in density) by the magnetic field in the vicinity of the heliopause. A similar effect is known for Earth's magnetopause (see [40]). This effect is related to an increase in the magnetic field component perpendicular to plasma motion when the plasma flow comes closer to the boundary of the flow region and, in particular, to the stagnation point. The magnetic field gradient then appears that decelerates the plasma. As a result, the flow changes such that the plasma starts flowing around the obstacle, a magnetic wall. This effect is clearly seen in Fig. 4. All three components of the magnetic field increase as they come closer to the heliopause (Fig. 4i–k). All three components of the velocity (Fig. 4e–g) and density (Fig. 4a) decrease when coming closer to the heliopause, starting from approximately the middle of the heliospheric shock layer. In this region, both the Alfvén Mach number and the plasma parameter β (defined as the ratio of the plasma pressure and the magnetic field pressure) become less than unity. This means that the magnetic field is the driving factor for the flow, i.e., the plasma distribution follows the field distribution. It is interesting that in the expulsion region, the magnetic field pressure 'expels' the plasma pressure such that the total pressure remains unchanged (Fig. 4b). The expulsion effect plays a significant role in a sufficiently large area of the

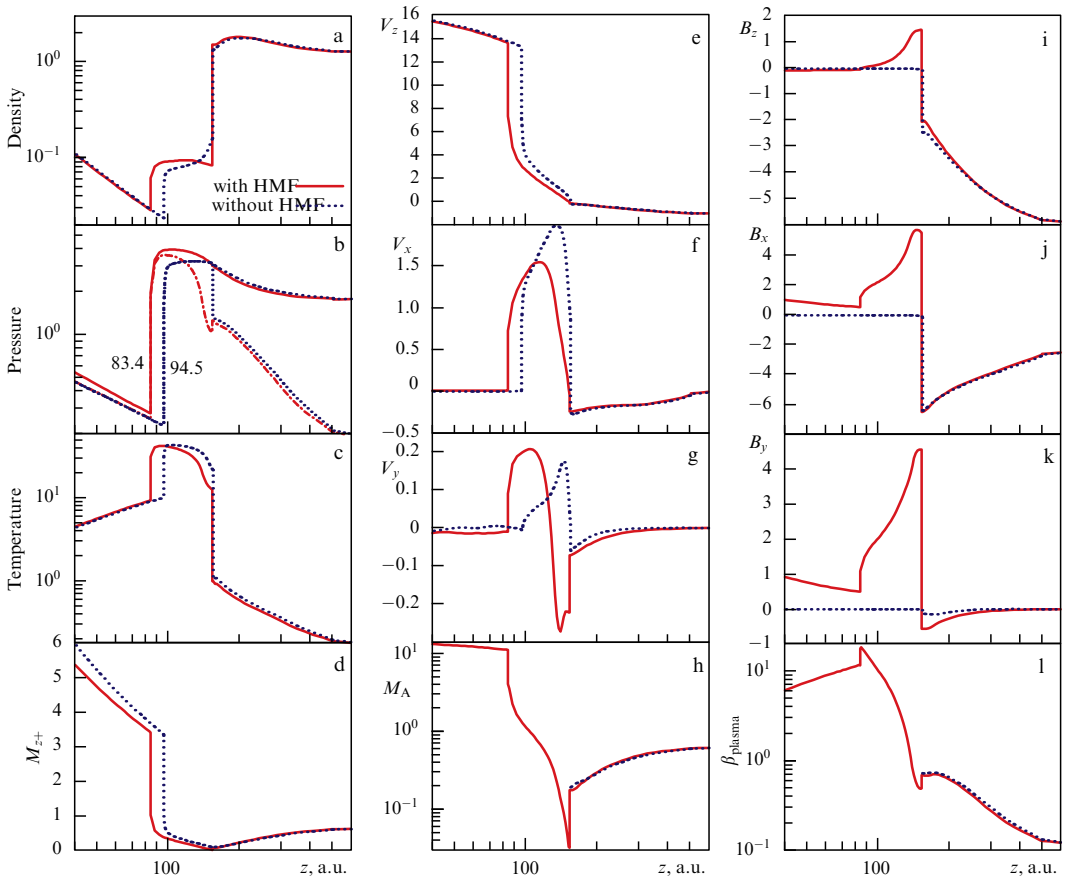

Figure 4. (a) Density, (b) static (dashed-dotted line) and total pressure, (c) temperature, and (e–g) velocity components of the plasma component and (i–k) the magnetic field component (relative units) as a function of heliocentric distance (plotted along the z axis). Solid curves correspond to the results of the model with the effect of the heliospheric magnetic field (HMF) taken into account, while dotted curves show the results with that effect ignored, (d) is the Mach number M_{z+} calculated using the fast magnetic sound speed, (h) is the Alfvén number M_A, and (l) is for the plasma parameter β.

heliosphere fore part, and the same effect results in a decrease in the heliocentric distance to the heliopause on the sides.

We note that the expulsion effect also gives rise to of a significant increase (by about a factor of 10) in density in crossing the heliopause. This result disagrees with the theoretical picture of a smooth (continuous) variation of plasma parameters at the heliopause in the vicinity of the stagnation point due to the charge-exchange effect (see [41]). A possible explanation for this disagreement is that the stagnation points inside and outside the heliopause do not coincide in a 3D geometry, while their coincidence is a prerequisite for the result obtained in [41].

The heliospheric magnetic field causes significant changes in plasma flow in the region of the heliospheric shock layer. A detailed analysis of the plasma flow along the heliopause is given in [25] (see Fig. 5 and comments on the figure). Importantly, another phenomenon is here related to the effect of the heliospheric magnetic field. This effect is currently under active discussion in the heliospheric community.

As follows from Parker's classical solution [33], at large heliocentric distances, the heliospheric magnetic field primarily has a toroid shape (the B_φ component dominates). Recent studies [42–44] have shown that if magnetized solar wind outflows into an interstellar medium at rest with counterpressure (in the absence of a magnetic field), the symmetry of the solar wind outflow breaks down, and two jets are formed around the Sun's rotation axis (see Fig. 1 in [43]). In [45], results of calculations of the global structure of the helio-

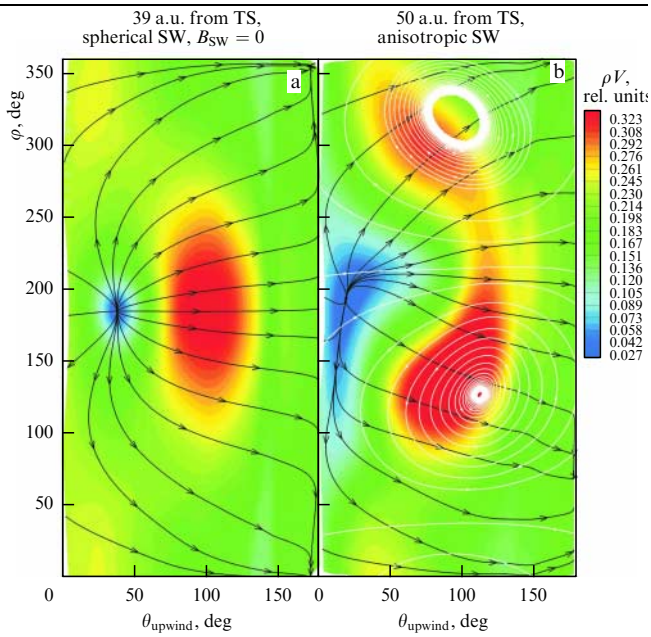

Figure 5. Mass flow (ρV) of the solar wind (SW) through a closed surface located in the region of the internal shock layer at an equal distance from the heliospheric shock wave. (Upwind is the direction opposite to the direction of the incoming flow of the interstellar medium.) The model results are presented (a) without and (b) with the heliospheric magnetic field taken into account. Dark lines show projections of the plasma component flow lines onto that surface and light lines show projections of the magnetic field lines.

sphere are presented, and jets are shown to also appear in the case of realistic boundary conditions in the interstellar medium. In this case, the heliopause has the shape of a curved tube.

The effect of the possible collimation of the solar wind into jets is to be reproduced in model [25], because it takes the effect of the heliospheric magnetic field into account. To show the effect of solar wind collimation toward the poles, the dependence of the mass flow (ρV) on the position on a closed surface located at some distance from the heliospheric shock wave is plotted in Fig. 5. The position on the closed surface is determined by two angles, one of which is measured from the direction toward the velocity vector of the interstellar medium flow (the z axis) and the other from the x axis (see the definition of the reference frame in Section 2.2.1). For calculations where the heliospheric magnetic field is disregarded (Fig. 5a), the flow maximum is observed in directions perpendicular to the motion of the interstellar medium $\theta \sim 100^\circ - 110^\circ$ and $\varphi \sim 180^\circ$. In those directions, the entire solar wind from the windward side is transported to the tail. The magnetic field produces two maxima: in the northern and southern hemispheres (Fig. 5b). These results are an indication that the effect of solar wind collimation toward the poles is present in the results of the model in [25]. However, this effect is not strong enough to drastically change the heliopause topology (at least in the area with a radius of 1,000–3,000 a.u. around the Sun). The difference between the results obtained and those in Ref. [45] is, in our opinion, explained by effects related to charge exchange of solar wind protons on interstellar hydrogen atoms, which ensure an effective exchange of momenta between the components. If there is a plasma stagnation point in the heliosphere tail part, the charge exchange causes that point to move away from the Sun to very large heliocentric distances, thus making the heliopause topology in the vicinity of the Sun undistinguishable from the 'classical' one.

2.2.4 Effect of heliolatitude dependence of solar wind parameters. Varying solar wind parameters with heliolatitude (see Fig. 2) results in an even more complex structure of the solar wind flow in the vicinity of the heliospheric shock layer. The heliolatitude dependence was shown in [25] not to result in qualitative changes in the global structure of the heliosphere and distribution parameters of the plasma component and magnetic field. Nevertheless, there are some quantitative differences. In particular, the heliopause shape grows blunter: in the direction of the incoming flow, the heliopause is closer to the Sun by $\sim 10-15$ a.u. (as compared to the spherically symmetric solar wind), while in the direction toward the poles, it stays farther away from the Sun by the same distance. This change in the heliopause shape is related to the nonmonotonic behavior of the dynamic pressure of the solar wind, which increases by 30–50% at medium latitudes and further decreases closer to the poles (see Fig. 2). The nonmonotonic dependence of the dynamic pressure on heliolatitude causes changes in the plasma flow in the region of the heliospheric shock layer and, in particular, a pressure decrease in the head part of the heliosphere.

The shape of the heliospheric shock wave changes in accordance with the heliopause shape; the distance to it also increases in the direction of the poles. We also note that because the heliopause is an obstacle for the interstellar medium flow, the changes in its shape affect interstellar plasma flow lines, and the changes in plasma distribution, in turn, affect the distribution of the hydrogen atoms produced in the heliopause vicinity due to charge exchange. It was shown in [25] that the V_x component of the velocity of atoms inside the heliosphere does change in calculations that take the heliolatitude dependence of the solar wind into account. This means that in analyzing data on scattered solar Lyman-alpha radiation, one should take the dependence of solar-wind parameters on the heliolatitude and solar cycle into account not only locally, inside the heliosphere (see [27]), but also in simulating the motion of atoms in the heliospheric interface region.

3. Comparing model results with experimental data

Prior to starting a comparison of model results with recently obtained space experiment data, the choice of external boundary conditions for the problem formulation has to be justified. Strictly speaking, there are four free parameters in the model that we consider: (1) the density of protons; (2) the density of interstellar hydrogen atoms; (3) the interstellar magnetic field strength; and (4) the interstellar magnetic field direction.

As we have noted, other parameters of the model are rather well known from space experiment data. In considering the four parameters, we assume that the magnetic field lies in the plane determined by the velocity vectors of the interstellar helium and hydrogen atoms. We note that as was shown in the model, this assumption holds only in an approximate way due to latitudinal variations of solar wind parameters. This circumstance definitely introduces some (minor) error into the estimates of other parameters.

Spacecraft data enable imposing essential constraints on both the free model parameters listed above and the characteristics of the interaction region to be described by the model. Below is a list of basic data.

(1) Distances to the heliospheric shock wave in the directions of the Voyager-1 and Voyager-2 spacecraft. Those values were directly determined when the spacecraft crossed the heliospheric wave at a distance of 83.7 and 94.1 a.u. in August 2004 and December 2007.

(2) Density of interstellar hydrogen atoms at heliocentric distances ($\sim 50-90$ a.u.), which is 0.10 ± 0.01 cm^{-3}. This value was obtained independently from an analysis of the distributions of captured protons measured in the solar wind (see, e.g., [47, 48]) and an analysis of the degree of deceleration of supersonic solar wind at large ($\sim 50-90$ a.u.) heliocentric distances due to the charge exchange of solar protons on interstellar hydrogen atoms (see [49]).

(3) Deviation of interstellar hydrogen atoms from the direction of motion of the interstellar medium not perturbed by the solar wind.

(4) Density and velocity of the solar wind in the regions of the heliocentric shock layer that were measured aboard Voyager-2 using the 'Plasma' device [50] (a similar device installed on Voyager-1 is unfortunately inoperable).

(5) Distance to the heliopause in the Voyager-1 direction. This distance, which is 122 a.u., was directly determined when Voyager-1 crossed the heliopause in late August and early September 2012 (see, e.g., [51]).

(6) Strength and direction of the magnetic field measured by the MAG device (magnetometer) installed aboard Voyager-1 in the region of the heliospheric shock layer [34].

(7) Estimated densities of protons in the interstellar medium obtained from the analysis of kHz range plasma waves measured by Voyager-1.

(8) Direction to the center of the belt of high-energy atoms of heliospheric origin that was discovered by the IBEX spacecraft [53]. In publications, this center is associated with the direction of the interstellar magnetic field [54].

The list of data pertaining to properties of the interstellar medium and heliospheric interface quoted above is not complete. For example, there is no information about measurements of high-energy particles by the Voyagers and IBEX in that list. Nevertheless, in conducting parametric studies, we come to the conclusion that within the model described above, it is not possible to attain good agreement of model results with the complete set of data using a single set of free parameters of the problem.

For example, it is impossible to reproduce (within the model with realistic boundary conditions) the distance (in the Voyager-1 direction) to the heliocentric shock wave equal to 94 a.u. and simultaneously the distance to the heliopause equal to 122 a.u. In the model in [25], as in similar models of other authors, the thickness of the shock layer in that direction is 50–70 a.u., which is significantly larger than the thickness of 28 a.u. determined by Voyager-1.

We note that although variations in solar wind parameters with the solar cycle result in fluctuations in the heliospheric wave location by 10 a.u. and in the heliopause location by 3–4 a.u. [21, 22], those fluctuations of discontinuity surfaces do not resolve the problem mentioned above. Because the shock wave thickness derived in the model is controlled by the mass, momentum, and energy conservation laws, we can significantly reduce it (by approximately a factor of two), only by adding to the model a physical process that would result in reducing pressure/energy in the shock layer region. For example, it was shown in [55] that taking electron heat conductivity into account results in diminishing thermal pressure in the layer and hence reducing its thickness.

To determine the values of the interstellar parameters, the analysis in [25] was restricted to the data specified in the first three items of the list above. This is explained by the model primarily used for analyzing data related to the neutral component (see [27, 56–58]). A parametric study has shown that the results of the model agree best with spacecraft data if the following values are adopted for the free parameters (and taken in setting up the problem): $n_{p,LISM} = 0.04$ cm^{-3}, $n_{H,LISM} = 0.14$ cm^{-3}, $B_{LISM} = 4.4$ μG, and $\alpha_{LISM} = 20°$.

The model described and its earlier versions were used to analyze data from various spacecraft. For example, in [59–65], the model was applied to analyzing absorption spectra of the Lyman-alpha radiation in the direction of nearest stars, which were measured by the Hubble Space Telescope. In particular, those studies have proved the existence of a so-called hydrogen wall, an increase in the interstellar atom density around the heliopause. This increase occurs as a result of charge exchange of interstellar hydrogen atoms with protons decelerated in the vicinity of the stagnation point on the heliopause. The secondary hydrogen atoms produced due to charge exchange have lower velocities (compared with those of primary atoms) and therefore accumulate in an area around the heliopause, thus forming a 'wall'. The existence of the hydrogen wall was theoretically predicted in [11, 66]. An analysis of the absorption spectra obtained by the Hubble Telescope also showed that similar walls probably exist around other stars, thus providing an additional option for studying properties of their stellar winds.

In many studies, the model of the heliospheric interface was used to analyze data on scattered solar Lyman-alpha radiation. A recent detailed review of those studies is available in [67].

The model was also used to analyze measurements of captured solar-wind ions [18, 19]. Those ions are produced within the heliosphere from interstellar atoms as a result of charge exchange and photo ionization. Their energy spectra have been measured by the Ulysses and ACE (Advanced Composition Explorer) spacecraft (with the SWICS (Solar Wind Composition Spectrometer) device) (see, e.g., [47]).

In a number of studies (see, e.g., [24, 46]), fluxes of high-energy hydrogen atoms were simulated and analyzed and the calculated results were compared with the IBEX data.

Not focusing on the results of earlier studies, we consider in more detail the analysis of interstellar oxygen fluxes measured by the IBEX spacecraft and scattered solar Lyman-alpha radiation that was done in [57, 58].

3.1 Measurements of secondary oxygen by the IBEX-Lo spacecraft

Interstellar atomic oxygen is the third most abundant element in the interstellar medium. Because the ionization energy of atomic oxygen is close to that of hydrogen, the cross section of charge exchange of oxygen atoms on protons is close to the resonance one: $H^+ + H = H + H^+$. It can therefore be expected that when oxygen atoms pass through heliospheric interface regions in the vicinity of the heliopause, an oxygen wall is produced, and both primary (interstellar) and secondary (produced in the vicinity of the heliopause in the process of charge exchange) oxygen atoms would penetrate into the heliosphere. The existence of secondary oxygen atoms was theoretically predicted in [68].

In [69], the first quantitative data on fluxes of interstellar oxygen atoms measured by IBEX were presented. In [57], the model [25] for solar-wind interaction with the local interstellar medium was used to calculate the fluxes of interstellar oxygen atoms, and the results obtained were compared with the IBEX data. For the data analysis to be correct, a model was used that enables describing the motion of interstellar atoms inside the heliosphere in detail and includes the temporal and heliolatitude dependence of the frequencies of ionization and charge exchange on solar-wind protons and the strength of solar gravitational attraction. The performed numerical simulation takes the actual geometry of IBEX spacecraft observations, technical specifications of the IBEX-Lo sensor, and the most recent results of gauging the device into account. Due to specific features of the sensor, the IBEX-Lo observations also included data on the flux of neon atoms that were also taken into account in calculations.

Figure 6a shows a map of the fluxes of neutral oxygen and neon atoms in elliptic coordinates, which is based on the IBEX-Lo sensor data, and Fig. 6b presents the results of corresponding numerical simulations. We see similar structures in both maps: from the main flux highlighted in red, a so-called tail stretches in the direction of smaller longitudes and larger latitudes. The calculated results show that the main flux is related to primary oxygen and neon atoms, while the tail represents fluxes of the secondary component of neutral oxygen atoms. These results confirm the theoretical prediction in [68] made in 1997.

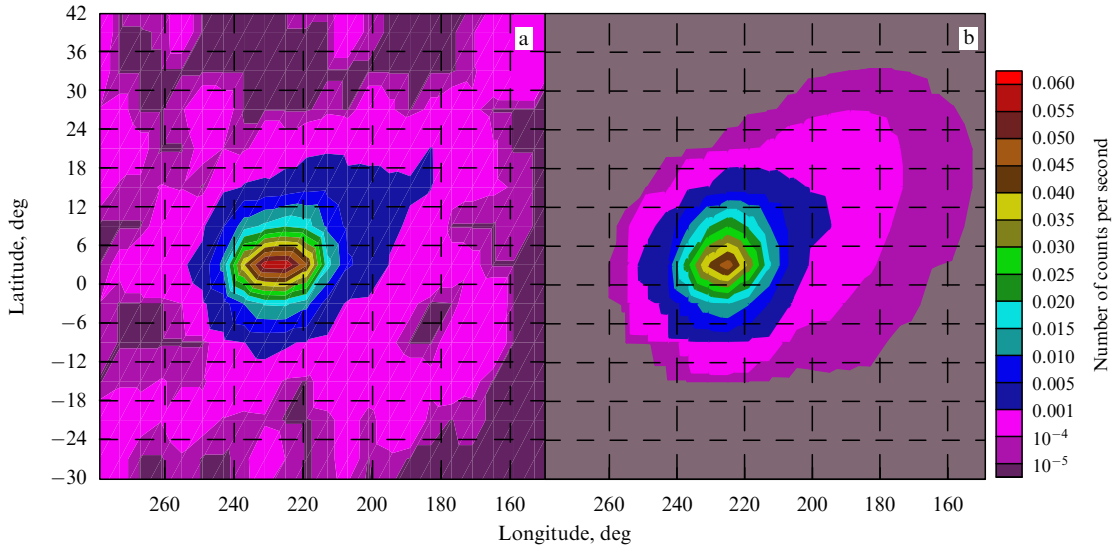

Figure 6. (Color online.) Comparison of (a) IBEX-Lo data with (b) the results of numerical calculations in energy channel 6. Subtracted from the map plotted using the IBEX-Lo data is the background flow $b_g = 2.32 \times 10^{-4}$ counts per second (see Table 3 in [69]). The chart is plotted in the heliocentric ecliptic reference frame (J2000).

3.2 Analysis of scattered solar Lyman-alpha radiation at large heliocentric distances

An interesting example of the model application that yielded a new and interesting result is the analysis of the intensity of scattered solar Lyman-alpha radiation in the outer heliosphere measured by Voyager-1 in 2003–2014 at distances of 90–130 a.u. from the Sun. At that time, the spacecraft was measuring the intensity of Lyman-alpha radiation in the direction that was nearly opposite to the oncoming flow of the interstellar wind. Because the spacecraft was moving all the time away from the Sun, the obtained data enable studying the dependence of the intensity of scattered solar Lyman-alpha radiation on the heliocentric distance.

Figure 7a shows the data obtained by Voyager-1 in 2003–2014. The intensity of the Lyman-alpha radiation scattered in the heliosphere is proportional to the flux of solar Lyman-alpha photons. Because we are interested in the processes that occur on the heliosphere boundary, it is reasonable to exclude solar flux variations from the data. To do so, we consider the ratio of the measured intensity to the solar flux in Earth's orbit. The intensity normalized in this way is shown in Fig. 7b. It can be seen that from 2003 to 2009, this intensity was virtually constant. A comparison of the normalized data with calculated results has shown that the model intensity monotonically decreases with increasing the distance from the Sun. This does not comply with the Voyager-1 data (Fig. 7b). In [58], two scenarios were proposed to explain those data. In the first scenario, one has to assume that there is constant background radiation of nonheliospheric origin. The intensity of that radiation should be of the order of 25 R (Fig. 7c). This additional radiation can be related to the galactic or extra-galactic background of Lyman-alpha radiation that can only be observed far from the Sun, where the heliospheric component becomes comparable to the extra-heliospheric one. An earlier recording of galactic Lyman-alpha radiation was reported in [70].

The second approach to explaining the Voyager-1 data is to assume that there is a condensed layer of hydrogen atoms located directly before or after the heliopause. Then the Lyman-alpha photons scattered on hydrogen atoms in the

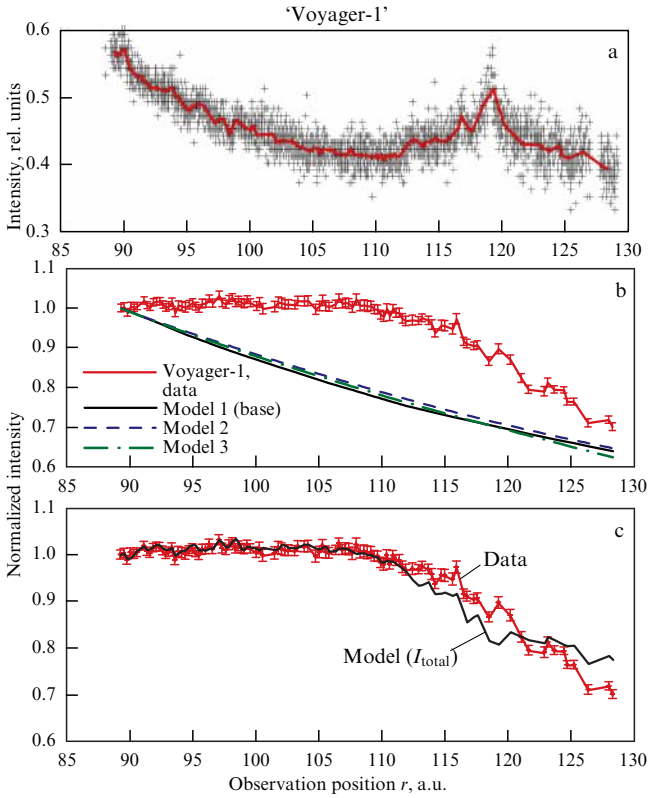

Figure 7. (Color online.) Intensity of Lyman-alpha radiation measured by Voyager-1 (the UVS device). (a) Intensity (red curve: data averaged over a 27-day interval). (b) Intensity normalized to the solar Lyman-alpha flux in Earth's orbit; comparison of Voyager-1 spacecraft data with the results of three models of the heliosphere boundary with different parameters (density of protons and hydrogen atoms) in the interstellar medium. (c) Comparison of the results of the model to which an extra-heliospheric radiation component with an intensity of 25 R is added, with Voyager-1 spacecraft data.

layer should have a significantly larger Doppler shift than that for the photons scattered on normal interstellar atoms, such that radiation is not absorbed by the heliosphere and can

be recorded by Voyager-1. In this case, the layer can be regarded as an additional permanent source of radiation for an observer coming close to the layer. After the observer has crossed the layer boundary, the intensity rapidly drops due to radiation absorption inside the layer. This layer was included into the model as an additional component of hydrogen atoms on which solar Lyman-alpha photons can scatter. The calculations have shown that the parameters of atoms in the layer must be approximately as follows: the density ~ 10 cm^{-3}, the velocity in the direction from the Sun ~ 50 km s^{-1}, and the temperature $\sim 10^4$ K. The physical nature of such a layer is currently unknown (see, however, [71]).

4. Conclusion

We have briefly described the main theoretical/model ideas regarding interaction of solar wind the with local interstellar medium. This interaction is shown to have a sophisticated multi-component nature. To obtain a theoretical description of the interaction region, kinetic magnetohydrodynamic models must be developed that take thermal components of solar-wind plasma and the interstellar medium into account, including interstellar hydrogen atoms described in a kinetic approach and suprathermal high-energy particles (both charged and neutral). Heliospheric and interstellar magnetic fields and the dependence of solar wind parameters on both time and heliolatitude should also be taken into account.

Numerical models of the heliosphere provide an explanation for a significant number of experimental data, including such model-sensitive data as the deviation of the direction of motion of interstellar hydrogen atoms from the direction of motion of the interstellar medium or the distance to the heliospheric shock wave in the directions toward the Voyager-1 and Voyager-2 spacecraft.

At the same time, the existing models fail to provide a consistent explanation (within the same model and the same set of parameters specifying the problem) of all data obtained by various spacecraft. For example, the measurements made by Voyager-1 indicate the probable existence of a dissipative process (for example, heat conductance) in the region of the heliospheric shock wave.

In our opinion, interest in studying the heliosphere boundary will only become stronger in the future. This interest will be primarily related to the endeavor to understand and provide a physical description of the data obtained from the Voyager-1 and Voyager-2 spacecraft and IBEX. New important information will appear when Voyager-2 crosses the heliopause, an event that is expected to occur in the nearest future.

Further investigations of the heliosphere boundary involve the Interstellar Probe [72], a new space project, and subsequent and more detailed studies of the heliosphere boundary from Earth's orbit or the L1 point (NASA's IMAP (Interstellar Mapper and Acceleration Probe) mission) [73].

Acknowledgments

The author is grateful to his colleagues D B Aleksashov, I I Baliukin, and O A Katushkina for joint studies. Results on global simulation of the heliosphere/astrospheres were obtained as part of the 14-12-01096 project of the Russian Science Foundation. The analysis of Lyman-alpha radiation, the results of which are presented in this paper, was partly supported by the Russian Foundation for Basic Research grant 16-52-16008.

References

1. Xu F, Borovsky J E *J. Geophys. Res. Space Phys.* **120** 70 (2015)
2. Katushkina O A et al. *Astrophys. J.* **789** 80 (2014)
3. McComas D J et al. *Astrophys. J. Suppl.* **220** 22 (2015)
4. Parker E N *Astrophys. J.* **134** 20 (1961)
5. Baranov V B, Krasnobaev K V, Kulikovskii A G *Sov. Phys. Dokl.* **15** 791 (1971); *Dokl. Akad. Nauk SSSR* **194** 41 (1970)
6. Bertaux J L, Blamont J E *Astron. Astrophys.* **11** 200 (1971)
7. Thomas G E, Krassa R F *Astron. Astrophys.* **11** 218 (1971)
8. Weller C S, Meier R R *Astrophys. J.* **193** 471 (1974)
9. Wallis M K *Nature* **254** 207 (1975)
10. Izmodenov V V *Astrophys. Space Sci.* **274** 55 (2000)
11. Baranov V B, Malama Y G *J. Geophys. Res.* **98** 15157 (1993)
12. Izmodenov V V et al. *Astrophys. Space Sci.* **274** 71 (2000)
13. Malama Y G *Astrophys. Space Sci.* **176** 21 (1991)
14. Myasnikov A V et al. *J. Geophys. Res. Space Phys.* **105** 5167 (2000)
15. Alexashov D B et al. *Astron. Astrophys.* **420** 729 (2004)
16. Izmodenov V *Space Sci. Rev.* **97** 385 (2001)
17. Izmodenov V V et al. *Astrophys. J. Lett.* **594** L59 (2003)
18. Izmodenov V V, Lallement R, Geiss J *Astron. Astrophys.* **344** 317 (1999)
19. Izmodenov V et al. *Astron. Astrophys.* **414** L29 (2004)
20. Izmodenov V V, Alexashov D B *Astron. Lett.* **29** 58 (2003)
21. Izmodenov V V, Malama Y G, Ruderman M S *Astron. Astrophys.* **429** 1069 (2005)
22. Izmodenov V V, Malama Y G, Ruderman M S *Adv. Space Res.* **41** 318 (2008)
23. Izmodenov V V, Alexashov D B, Myasnikov A V *Astron. Astrophys.* **437** L35 (2005)
24. Izmodenov V V et al. *Space Sci. Rev.* **146** 329 (2009)
25. Izmodenov V V, Alexashov D B *Astrophys. J. Suppl.* **220** 32 (2015)
26. Malama Y G, Izmodenov V V, Chalov S V *Astron. Astrophys.* **445** 693 (2006)
27. Katushkina O A, Izmodenov V V, Alexashov D B *Mon. Not. R. Astron. Soc.* **446** 2929 (2015)
28. Lindsay B G, Stebbings R F *J. Geophys. Res. Space Phys.* **110** A12213 (2005)
29. Sokól J M et al. *Solar Phys.* **285** 167 (2013)
30. Quémerais E et al. *J. Geophys. Res. Space Phys.* **111** A09114 (2006)
31. Lallement R et al. *AIP Conf. Proc.* **1216** 555 (2010)
32. Katushkina O A et al *J. Geophys. Res. Space Phys.* **118** 2800 (2013)
33. Parker E *Astrophys. J.* **128** 664 (1958)
34. Burlaga L F, Ness N F *Astrophys. J. Lett.* **744** A51 (2012)
35. Witte M *Astron. Astrophys.* **426** 835 (2004)
36. Bzowski M et al. *Astron. Astrophys.* **569** A8 (2014)
37. Wood B E, Müller H R, Witte M *Astrophys. J. Lett.* **801** 62 (2015)
38. Izmodenov V V *Space Sci. Rev.* **143** 139 (2009)
39. Lallement R *Science* **307** 1447 (2005)
40. Zwan B J, Wolf R A *J. Geophys. Res.* **81** 1636 (1976)
41. Belov N A, Ruderman M S *Mon. Not. R. Astron. Soc.* **401** 607 (2010)
42. Drake J F, Swisdak M, Opher M *Astrophys. J. Lett.* **808** L44 (2015)
43. Golikov E A et al. *Mon. Not. R. Astron. Soc.* **464** 1065 (2017)
44. Golikov E A et al. *J. Phys. Conf. Ser.* **815** 012035 (2017)
45. Opher M et al. *Astrophys. J. Lett.* **800** L28 (2015)
46. Chalov S V et al. *Astrophys. J. Lett.* **716** L99 (2010)
47. Geiss J, Gloeckler G, Fisk L, in *The Physics of the Heliospheric Boundaries* (ISSI Scientific Reports Series, Vol. 5, Eds V V Izmodenov, R Kallenbach) (Frascati: ESA, 2006) p. 137
48. Bzowski M et al. *Astron. Astrophys.* **491** 7 (2008)
49. Richardson J D et al. *Astron. Astrophys.* **491** 1 (2008)
50. Burlaga L F et al. *Astrophys. J.* **818** 147 (2016)
51. Cummings A C et al. *Astrophys. J.* **831** 18 (2016)
52. Gurnett D A et al. *Science* **341** 1489 (2013)
53. McComas D J et al. *Science* **326** 959 (2009)
54. Funsten H O et al. *Astrophys. J. Lett.* **776** 30 (2013)
55. Izmodenov V V, Alexashov D B, Ruderman M S *Astrophys. J. Lett.* **795** L7 (2014)
56. Katushkina O A et al. *Astrophys. J. Suppl.* **220** 33 (2015)
57. Baliukin I I et al. *Astrophys. J.* **850** 119 (2017)
58. Katushkina O A et al. *J. Geophys Res. Space Phys.* **122** 10921 (2017)
59. Izmodenov V V, Lallement R, Malama Y G *Astron. Astrophys.* **342** L13 (1999)

60. Izmodenov V, Wood B, Lallement R *J. Geophys. Res. Space Phys.* **107** 1308 (2002)
61. Wood B E et al. *Adv. Space Res.* **34** 66 (2004)
62. Wood B E et al. *Astrophys. J.* **657** 609 (2007)
63. Wood B E et al. *Astrophys. J.* **659** 1784 (2007)
64. Wood B E, Izmodenov V V, Malama Y G *Space Sci. Rev.* **143** 21 (2009)
65. Wood B E et al. *Astrophys. J.* **780** 108 (2014)
66. Baranov V B, Lebedev M G, Malama Y G *Astrophys. J.* **375** 347 (1991)
67. Izmodenov V V et al., in *Cross-Calibration of Far UV Spectra of Solar System Objects and the Heliosphere* (ISSI Scientific Report Series, Vol. 13) (New York: Springer, 2013) p. 7
68. Izmodenov V V, Lallement R, Malama Y G *Astron. Astrophys.* **317** 193 (1997)
69. Park J et al. *Astrophys. J. Suppl.* **220** 34 (2015)
70. Lallement R et al. *Science* **334** 1665 (2011)
71. Lallement R et al. *Astron. Astrophys.* **563** A108 (2014)
72. McNutt R L (Jr.) et al. *Acta Astronautica* **69** 767 (2011)
73. Schwadron N A et al. *J. Phys. Conf. Ser.* **767** 012025 (2016)